PARAMETER ANALYSIS OF A SINGLE STAGE INDUCTION MASS DRIVER

J. Bernardes and S. Merryman
Naval Surface Weapons Center
Dahlgren, Virginia 22448-5000

ABSTRACT

The electromechanical behavior of a Single Stage Induction Mass Driver (SSIMD) has been modeled and analyzed with the aid of a computer. The analysis focused on the effects of circuit parameters on projectile velocity and system efficiency. A description of the model along with general rules for the design of efficient SSMID systems are presented.

INTRODUCTION

The promise of achieving high velocities and high efficiencies has made the SSIMD an attractive concept for many applications. Since the mid-sixties the SSIMD has been adapted to such applications as: magnetic flux compressors {1}, hypervelocity mass accelerators {2}, induction reaction engines {3},{4}, and electromagnetic metal formers {5}.

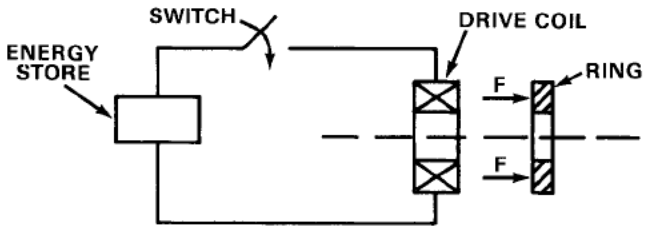

Figure 1: Single Stage Induction Mass Driver

The generic SSIMD (figure 1) basically consists of an energy storage (normally a capacitor bank), a switch, a drive coil, and a driven ring. The coil and ring are concentric and typically of equal diameter (the condition for maximum magnetic coupling). When a current pulse is applied to the drive-coil, a current is magnetically induced in the ring. The interaction between this ring current and the magnetic field (between the coil and the ring) produces a Lorentz Force which drives the ring.

The ring and coil geometries, and their relative orientation vary depending on the desired drive-direction (figure 2). In figure 2a the ring is driven axially, away from the drive coil. This is the geometry normally used in reaction engines and hypervelocity accelerators. In figure 2b the ring is driven inward radially, making this coil-ring arrangement favorable for flux-compression and metal forming applications.

In an effort to explore efficient induction driving, a twin capacitor bank system has been built and computer simulated. This twin bank scheme allows the use of high energy-density capacitors (for a compact system) by preventing voltage reversal across the banks. This paper is based mainly on experimental and simulation work with the above system.

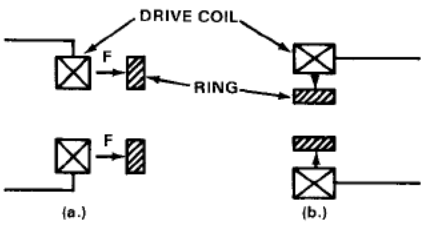

Figure 2: The two basic drive system geometries, a. typical geometry of axial accelerators b. typical geometry of flux compressors and metal formers

CIRCUIT MODEL

Our system has been electrically modeled by the circuit shown in figure 3. For discussion purposes, the circuit has been divided into two main sections: (1) the drive system, which includes the drive coil and the ring; and (2) the power system, which includes the capacitor banks, the switch and the power bus.

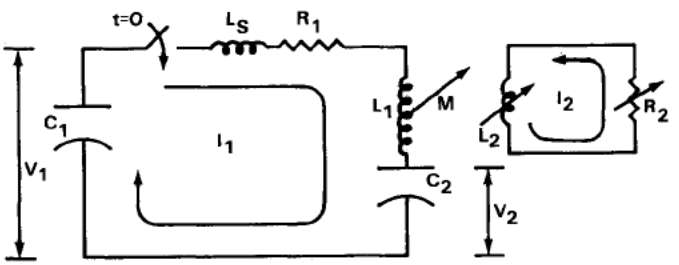

Figure 3: Circuit model of twin capacitor-bank device

The drive system has been modeled as a transformer with a shorted secondary and a mutual inductance (M) which is a function of ring separation. The self inductance of the primary (L_1) is the drive coil inductance. This value is proportional to the coil mean diameter and the number of turns squared. The secondary self inductance (L_2) is the ring inductance, which, within a few percent can be approximated by {6}

$$L_2=\mu_o R_m\{\ell n(\frac{R_m}{w})+.9\} \quad (1)$$

Where R_m is the ring's mean radius and w is its width. L_2 is a variable quantity if ring deformation occurs during acceleration. Due to the typically high turns ratio between the primary and the secondary, the ring sees the highest currents in the system, and therefore experiences significant heating. For this reason, R_2, the ring resistance, is modeled as a temperature dependent element defined by the following equation:

$$R_2=R_{2o}\{1+K_t(T-T_o)\} \quad (2)$$

Report Documentation Page

Form Approved
OMB No. 0704-0188

1. REPORT DATE	2. REPORT TYPE	3. DATES COVERED
JUN 1985	**N/A**	**-**

4. TITLE AND SUBTITLE	5a. CONTRACT NUMBER
Parameter Analysis Of A Single Stage Induction Mass Driver	5b. GRANT NUMBER
	5c. PROGRAM ELEMENT NUMBER
6. AUTHOR(S)	5d. PROJECT NUMBER
	5e. TASK NUMBER
	5f. WORK UNIT NUMBER
7. PERFORMING ORGANIZATION NAME(S) AND ADDRESS(ES) **Naval Surface Weapons Center Dahlgren, Virginia 22448-5000**	8. PERFORMING ORGANIZATION REPORT NUMBER
9. SPONSORING/MONITORING AGENCY NAME(S) AND ADDRESS(ES)	10. SPONSOR/MONITOR'S ACRONYM(S)
	11. SPONSOR/MONITOR'S REPORT NUMBER(S)

12. DISTRIBUTION/AVAILABILITY STATEMENT
Approved for public release, distribution unlimited

13. SUPPLEMENTARY NOTES
See also ADM002371. 2013 IEEE Pulsed Power Conference, Digest of Technical Papers 1976-2013, and Abstracts of the 2013 IEEE International Conference on Plasma Science. Held in San Francisco, CA on 16-21 June 2013. U.S. Government or Federal Purpose Rights License.

14. ABSTRACT
The electromechanical behavior of a Single Stage Induction Mass Driver (SSIMD) has been modeled and analyzed with the aid of a computer. The analysis focused on the effects of circuit parameters on projectile velocity and system efficiency. A description of the model along with general rules for the design of efficient SSMID systems are presented.

15. SUBJECT TERMS

16. SECURITY CLASSIFICATION OF:			17. LIMITATION OF ABSTRACT	18. NUMBER OF PAGES	19a. NAME OF RESPONSIBLE PERSON
a REPORT	b ABSTRACT	c THIS PAGE			
unclassified	**unclassified**	**unclassified**	**SAR**	**4**	

Where K_t is the temperature coefficient of the ring-material (for copper and aluminum, at 20 °C, K_t=.0039 {7}), T_o is the initial ring temperature, T is the operating temperature, and R_{2o} is the initial ring resistance -defined by

$$R_{2o}=\frac{2\pi R_m}{CwT_h} \tag{3}$$

where C is the ring-conductivity, and T_h is the ring thickness. The separation dependent mutual inductance, M, is determined using the following semiempirical procedure: First, the drive system circuit is transformed, ignoring R_2, to its T-model equivalent (figure 4).

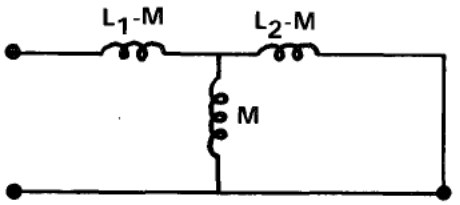

Figure 4: T-model of drive system used to obtain M(z)

From this circuit, the effective drive system inductance, L_{eff}, (measured at the primary terminals) is

$$L_{eff}=L_1-\left(\frac{M^2}{L_2}\right) \tag{4}$$

or

$$M=\sqrt{L_2(L_1-L_{eff})} \tag{5}$$

By measuring L_{eff} at increments of ring-coil normal separation, z, curves for L_{eff} and M, similar to the ones in figure 5, are obtained.

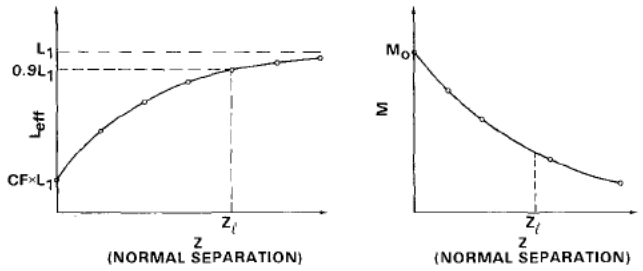

Figure 5: Experimental curves for drive system effective inductance and mutual inductance (coil mean diameter =20.5 cm, 6 turns)

Finally, an exponential curve fit to the discrete M(z) and $L_{eff}(z)$ yields the following expressions

$$L_{eff}=L_1\{1-(\frac{L_{2o}}{L_2})Ko^2e^{-2z/z_\ell}\} \tag{6}$$

$$M=\sqrt{L_{2o}L_1}\,K_o e^{-z/z_\ell} \tag{7}$$

where K_o is the initial (at z=0) coupling coefficient (as used in transformer terminology) and is defined by

$$K_o=\sqrt{1-C_f} \tag{8}$$

where C_f, the compensation factor, is the factor by which L_1 is reduced when the ring is at z=0. Z_ℓ, the coupling length, is the separation up to which there is significant coil-ring magnetic interaction, and it is defined as the separation when L_{eff}=.9L_1. This coupling length has experimentally been found to roughly equal .17D, where D is the mean drive-coil diameter. This result agrees with streak camera observations by Bondaletov {2} of the maximum separation up to which the ring is accelerated.

In the power-system, R_1 is the lumped representation of the primary loop resistance, and it is obtained from the exponential decay of the oscillating primary current (I_1) without the ring in place. Similarly, the stray inductance, L_s, is obtained from the oscillating frequency of I_1 when the coil is replaced by a shorting strap. Finally, C_1 and C_2 represent two capacitor banks of equal capacitance; where initially C_1 is charged and C_2 is uncharged.

SIMULATION

In order to predict the behavior of our SSIMD, a computer simulation has been developed using the circuit model previously described. The time behavior of the following variables were of interest: the primary current (I_1), the secondary (ring) current (I_2), the capacitor banks voltages (V_1 and V_2), the ring's normal velocity (v), the normal force exerted on the ring (F), the normal ring position (z), and the heat energy dissipated in the ring (E_2). The approach taken was to first write differential loop equations for the primary and the secondary of figure 3, and then manipulate them into a form that could be solved numerically. For the primary

$$L_1\dot{I}_1+I_1R_1+Q_2/C_2-Q_1/C_1+M\dot{I}_2+I_2\dot{M}=0 \tag{9}$$

and the secondary

$$(\dot{L}_2+R_2)I_2+L_2\dot{I}_2+M\dot{I}_1+I_1\dot{M}=0 \tag{10}$$

Where Q_1 and Q_2 are respectively the charge stored in C_1 and C_2. The numerical technique used was a fourth order Runge-Kuta Method, which requires that the derivative of the variable to be solved be equal to an expression which does not include that derivative. By respectively multiplying equations (9) and (10) by L_2 and M, then subtracting the resultant equations an expression for dI_1/dt is obtained

$$\dot{I}_1=\frac{1}{L_2L_1-M^2}\{Q_1L_2/C_1-L_2Q_2/C_2+(M\dot{M}-L_2R_1)I_1 + (M\dot{L}_2+R_2M-L_2\dot{M})I_2\} \tag{11}$$

Similarly, by respectively multiplying equations (9) and (10) by M and L_1, and then subtracting the resultant equations dI_2/dt is obtained

$$\dot{I}_2=\frac{1}{L_2L_1-M^2}\{MQ_2/C_2-MQ_1/C_1+(MR_1-\dot{M}L_1)I_1 + (M\dot{M}-L_1\dot{L}_2-R_2L_1)I_2\} \tag{12}$$

The rest of the necessary equations are:

$$\dot{Q}_1=-I_1 \tag{13}$$

where

$$V_1=V_o+Q_1/C_1 \tag{14}$$

$$Q_2 = I_1 \tag{15}$$

where

$$V_2 = Q_2 / C_2 \tag{16}$$

The force exerted on the ring is defined by {8}

$$F = I_1 I_2 dM/dz \tag{17}$$

or

$$\dot{v} = F/m = (I_1 I_2/m)(dM/dz) \tag{18}$$

where m is the mass of the ring.

$$\dot{z} = v \tag{19}$$

and

$$\dot{E}_2 = I_2^2 R_2 \tag{20}$$

Figure 6 shows the various simulation output curves for a sample run along with comparable measured variables.

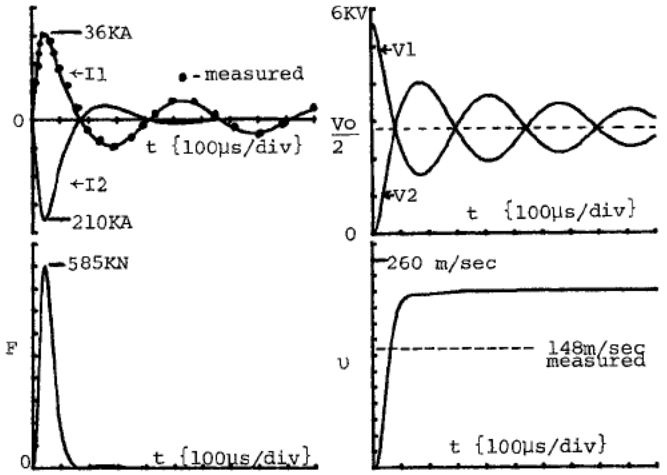

Figure 6: Computer generated curves compare to measurements for the following case: L_1=14μH, C_1=C_2=828μF, R_1=34mΩ, L_s=1μH, Z_ℓ=.035m, L_{2o}=.32μH, R_{2o}=.65mΩ, m=.115 Kg, and K_o=.89

In general, good agreement exists between measured and calculated values. The most signficant error exists in the velocity prediction (typically by a factor of ~.7). This error is probably due to aerodynamic effects which have not been modeled.

ANALYSIS

In an effort to emperically develop rules for the design of energy efficient SSIMD, the previously described simulation was used to generate the family of curves shown in figure 7.

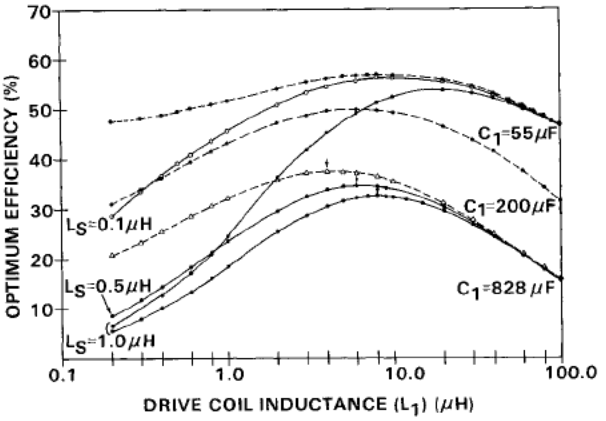

Figure 7: Computer generated optimum efficiency curves as a function of L_1, C_{eff}, and L_s. R_1=15.6mΩ, R_2=1.1mΩ, L_2=.32μH, K_o=.89, Z_ℓ=.035m, and m=.1 Kg

The solid and dashed curves respectively represent the presence and absence of stray inductance in the system, and have been generated for three values of C_1 (C_2=C_1).

Each point in these curves represents an optimum efficiency for a given set of circuit elements, and was found by stepping through the charge voltage until an efficiency maximum was reached. The purpose of changing the voltage was to vary the ring velocity. These points agree with the following criterion {4}:

$$\langle v \rangle = z_\ell / \langle T/2 \rangle \tag{21}$$

where $\langle v \rangle$ is the average ring velocity and $\langle T/2 \rangle$ is the average first half-period of the primary current - defined by

$$\langle T/2 \rangle = \pi \sqrt{\langle L_{eff} \rangle C_{eff}} \tag{22}$$

where

$$\langle L_{eff} \rangle = \frac{1}{z_\ell} \int_0^{z_\ell} L_{eff}\, dz + L_s \tag{23}$$

and C_{eff} is the effective system capacitance. For example, in the twin capacitor bank system C_{eff} equals the series combination of C_1 and C_2. The above criterion simply states that in order to drive a ring most efficiently, the ring must remain in the coupling region (between z=0 and $z=Z_\ell$) for exactly $\langle T/2 \rangle$.

By comparing the solid and dashed curves the adverse effects of stray inductance on efficiency is clearly seen. When L_s is of the order of L_1 a signficant energy division occurs between the two: this division reduces the amount of energy available at the drive coil, and consequently reduces drive efficiency. Aside from the effects of L_s on efficiency, when L_1 is made too small, the efficiency is also reduced, as shown by the dashed curves of figure 7. This effect can be attributed to the effective coupling parameter $dM/dz|_{eff}$, which is present in the force equation, as shown below

$$F=I_1 I_2 dM/dz=I_1^2 M/L_2 dM/dz=I_1^2 dM/dz\Big|_{eff} \quad (24)$$

This effective coupling parameter is used as a figure of merit when comparing difference induction accelerators {4}. The dependence of $dM/dz|_{eff}$ on L_1 can be seen when M and dM/dz are spacially averaged from, z=0 to Z_ℓ and substituted into eqn. (24)

$$\left\langle \frac{dM}{dz}\right|_{eff} \rangle = \frac{.4K_o^2 L_1}{z_\ell} \quad (25)$$

Although it is undesirable for L_1 to be small, it is also undesirable for it to be too large, since I_1, (the other term in eqn. (24)), will be reduced.

These curves also show the beneficial effects, in terms of efficiency, of reducing the effective system capacitance. Since lower capacitance translates to higher velocity (from the optimum efficiency criteria), the trends in figure 7 imply that induction drivers have a natural tendency to efficiently drive rings to high velocities. Unfortunately, the price paid for reducing the capacitance and still operate at optimum efficiency is an increase in charge voltage, which ultimately becomes one of the practical limits on device performance. This voltage limit is approximately 100Kv {4}. An estimate of the optimum charge voltage, which agrees with the simulation results, can be derived from the force equation (eqn. (17)) by averaging all of the pertinent variables: if $L_2/R_2 >> < T/2>$, which usually is the case, eqn. (17) can be rewritten as

$$F=I_1^2 (M/L_2) dM/dz=ma \quad (26)$$

Averaging this expression and replacing <a> , the average ring acceleration, with $<v>/<T/2>$

$$(2m<v>)/<T/2>=I_p^2/4<M/L_2 (dM/dz)> \quad (27)$$

where I_1 was replaced by its RMS value from t=0 to $t=<T/2>$, $Ip/\sqrt{4}$. I_p is the peak primary current, defined by

$$I_p=V_o\sqrt{\frac{C_{eff}}{<L_{eff}>}} \quad (28)$$

Finally, combining eqns. (25) and (26) yields an expression for the optimum charge voltage.

$$V_o=\sqrt{\frac{4m<v>}{\pi}\frac{\sqrt{<L_{eff}>}}{(C_{eff})^{1.5}<\frac{M}{L_2}\frac{dM}{dz}>}} \quad (29)$$

The curves in figure 7 are independent of ring mass, but the charge voltage required to operate at optimum efficiency is proportional to the square root of the mass -as indicated by Eqn. (29).

DESIGN PROCEDURE

The purpose of this procedure is to determine the values of the circuit elements and the charge voltage, based on a design velocity and drive system dimensions, which will yield an efficient SSIMD. The objective is to choose the circuit parameters which will cause the device to operate near the optimum efficiency peaks of figure 7. The procedure assumes a capacitive discharge, series RLC-circuit; and a drive-coil and ring of roughly equal diameter. The first step is to minimize the values of L_s and R_1. L_s is determined by the geometry of the power system; some typical low values for parallel plate and coaxial geometries are respectively 250nH{3} and 120nH 4 (at voltages near 30Kv). R_1 is the conductor resistance of the primary circuit, and is typically of the order of 10E-3 ohms. The application normally dictates the dimensions of the drive-coil and the ring. These dimensions in turn determine L_2 and the lower limit of L_1. By increasing the number of turns, L_1 is increased until $L_1 > 10L_s$. The upper limit on L_1 is not easily defined, and it may be necessary to use a computer model to determine its optimum value. R_2 is determined by the ring's dimensions and material properties. This parameter has a strong impact on efficiency through the $I_2^2R_2$ loses, and therefore should be minimized. C_{eff} is chosen according to the optimum efficiency criteria (eqn. (21)), where the average velocity can be approximated by one half the design velocity. Finally, a rough estimate of the required voltage is obtained using eqn. (29), where the spacial averages for M, L_{eff}, and dM/dz are found from their previously described equations.

REFERENCES

{1} S. Chikazumi, et. al., "Production of Magnetic Fields in Megagauss Region and Related Measuring Techniques," IEEE Trans. on Magnetics, Vol. MAG-14, Mo.5, pp 577-585, Sep 78.

{2} V.M. Bondaletov and E.M. Ivanov, "Ultra High Axial Acceleration of Conducting Rings," Sov. Phys. Tech. Phys., Vol. 22, Mo. 2, February 1977.

{3} R.H. Lovberg and C.L. Dailey," Large Inductive Thruster Performance Measurement," 15th International Electric Propulsion Conference, Las Vegas, Nev. April 21-23, 1981.

{4} P. Mongeau, "Single Stage Pulsed Induction Reaction Engine," Mass. Inst. of Tech., Cambridge, Mass.

{5} J.R. Bennett and M.M. Plum, "Electromagnetic Forming-An Industrial Application of Pulse Power," Pulsed Power Lecture Series, No. 36, 1981.

{6} C.L. Dailey and R.H. Lovberg, "Large Diameter Inductive Plasma Thrusters," Princeton/AIAA/DGLR 14th International Electric Propulsion Conference, Princeton, NJ, Oct. 30-Nov. 1, 1979.

{7} P. Mongeau, "Coaxial Aircore Electromagnetic Accelerators," Mass. Inst. of Tech., Cambridge, Mass., October 19.

{8} H.H. Kolm, "Basic Coaxial Mass Driver Reference Design," Mass. Inst. of Tech., Cambridge, Mass, 1977.